

## THE METASOMATIC CHANGES THAT ACCOMPANY URANIUM MINERALIZATION IN THE NONOROGENIC RHYOLITES OF THE UPPER AILLIK GROUP, LABRADOR

MICHAEL V.W. WHITE

*X-Plor International Corporation, 20 Speers Road, Suite 706, Oakville, Ontario L6K 3R5*

ROBERT F. MARTIN

*Department of Geological Sciences, McGill University,  
3450 University Street, Montreal, Quebec H3A 2A7*

### ABSTRACT

The porphyritic rhyolites and tuffs of the Upper Aillik Group (Labrador) contain clear textural and mineralogical signs of very low pressure crystallization; their compositional characteristics suggest that they are products of highly evolved granitic melts of nonorogenic affinity. The tuffs, originally mostly glassy, probably were enriched in alkalis, uranium, thorium and a host of incompatible elements. However, these primary concentrations have been disturbed, especially in the finer grained tuffaceous rocks, by autometasomatic reactions: (1) K-metasomatism, not associated with disruption of primary U/Th ratios; (2) Na-metasomatism and desilication, probably at higher temperatures than (1) and associated with important uranium mineralization in a mildly peralkaline environment (*e.g.*, Michelin ore zone). The feldspar textures and mineralogy provide insight into the direction of metasomatic enrichment. Zr, Pb, CO<sub>2</sub>, Cl and F increased and Th, Cu and S decreased with desilication; the dominant metasomatic trends recall fenitization-type reactions. The mobilization of the residual elements probably accompanied devitrification of glass shards and pumice fragments in the ash. Rock-fluid interaction may have been long-lived, as the ignimbrites and plugs may have been surface expressions of an epizonal granitic complex. Distinctly later orogenies may have been important factors in the development of economic concentrations of uranium.

**Keywords:** uranium, thorium, Upper Aillik Group, Labrador, nonorogenic, desilication, metasomatism, alkali exchange, alkali feldspars.

### SOMMAIRE

Les tufs et les porphyres rhyolitiques de la partie supérieure du groupe Aillik (Labrador) contiennent des signes clairs, de par leur texture et leur minéralogie, de cristallisation primaire de liquides granitiques non-orogéniques à très basse pression. Originellement composés surtout de particules vitreuses, les tufs étaient probablement riches en alcalins, uranium, thorium et autres élé-

ments incompatibles. Cependant, ces concentrations primaires ont été modifiées, surtout dans les tufs, vu leur granulométrie fine, par les réactions autométasomatiques suivantes: (1) métasomatisme K, qui n'a pas causé de disruption dans les rapports U/Th primaires; (2) métasomatisme Na et désilication, probablement à plus haute température que (1) et associés à une importante minéralisation en uranium dans un milieu devenu légèrement hyperalcalin (dans la zone minéralisée de Michelin, par exemple). Texture et minéralogie des feldspaths contribuent à identifier la direction des transformations métasomatiques. Zr, Pb, CO<sub>2</sub>, Cl et F ont augmenté, tandis que Th, Cu et S ont diminué, au cours de la désilication; l'allure dominante du métasomatisme rappelle les réactions de fenitisation. La mobilisation des éléments résiduels a probablement accompagné la dévitrification d'esquilles de verre et de fragments de ponce dans les tufs. L'interaction des roches avec l'eau a pu être de longue durée, pour autant que les ignimbrites et les dômes à noyau de percement soient des manifestations de surface d'un complexe granitique de l'épizone. Des orogénèses tardives peuvent, elles aussi, avoir contribué au développement des concentrations économiques d'uranium.

**Mots-clés:** uranium, thorium, groupe de l'Aillik supérieur, Labrador, non-orogénique, désilication, métasomatisme, échange d'alcalins, feldspaths alcalins.

### INTRODUCTION

The Aphebian and later Proterozoic metasedimentary and metavolcanic rocks found exposed in a belt southwest of the Makkovik Bay - Kaipokok Bay area, southern Labrador, are of considerable economic interest because they host a number of uranium showings. These occur in four groupings that define the Central Mineral Belt (Kontak *et al.* 1980a). Gandhi (1978) has summarized the geological setting and genetic aspects of the disseminated and vein-type pitchblende deposits, and Evans (1980) has recently focused on the geology and geochemistry of

deposits in the Kitts – Post Hill and Michelin – Burnt Lake belts. The deposits in the Michelin – Burnt Hill belt are found in tuffaceous felsic volcanic rocks and associated volcanogenic sediments that constitute the upper part of the Aillik Group (Aphebian,  $1770 \pm 4$  Ma; Kontak *et al.* 1980b). Rocks of the Aillik Group have been intruded by granitic, syenitic and gabbroic rocks that in many instances seem to have escaped the effects of Hudsonian deformation; one such case is the Walker Lake granite ( $1550 \pm 55$  Ma; Kontak *et al.* 1980b). Some of these intrusive bodies define associations that are typically nonorogenic [Martin & Piwinski 1972; *e.g.*, the syenites, gabbros and pyroxenites of the Adlavik complex (Bailey *et al.* 1979), the Walker Lake granite (by implication), and the Paleohelikian alkali granite –

alkali syenite – diorite complex of the Benedict Mountains (Gower 1980)]. However, the Aillik Group and some intrusive complexes definitely were affected by the Hudsonian orogeny (Sutton *et al.* 1972, Clark 1979). Near Kaipokok Bay, up to three distinct phases of deformation can be recognized in the folded sequence (Clark 1971, Marten 1977). Uranium mineralization predates at least the final phase of Hudsonian deformation (Gandhi 1978), such that a good case can be made for a close association of the uranium with Aillik felsic volcanism. We concur with Gandhi's statement that the deposits are related to volcanic processes; note, however, that in a recent review of uranium occurrences in Canada, McMillan (1978) attributed a purely sedimentary origin to U deposits in the Central Mineral Belt.

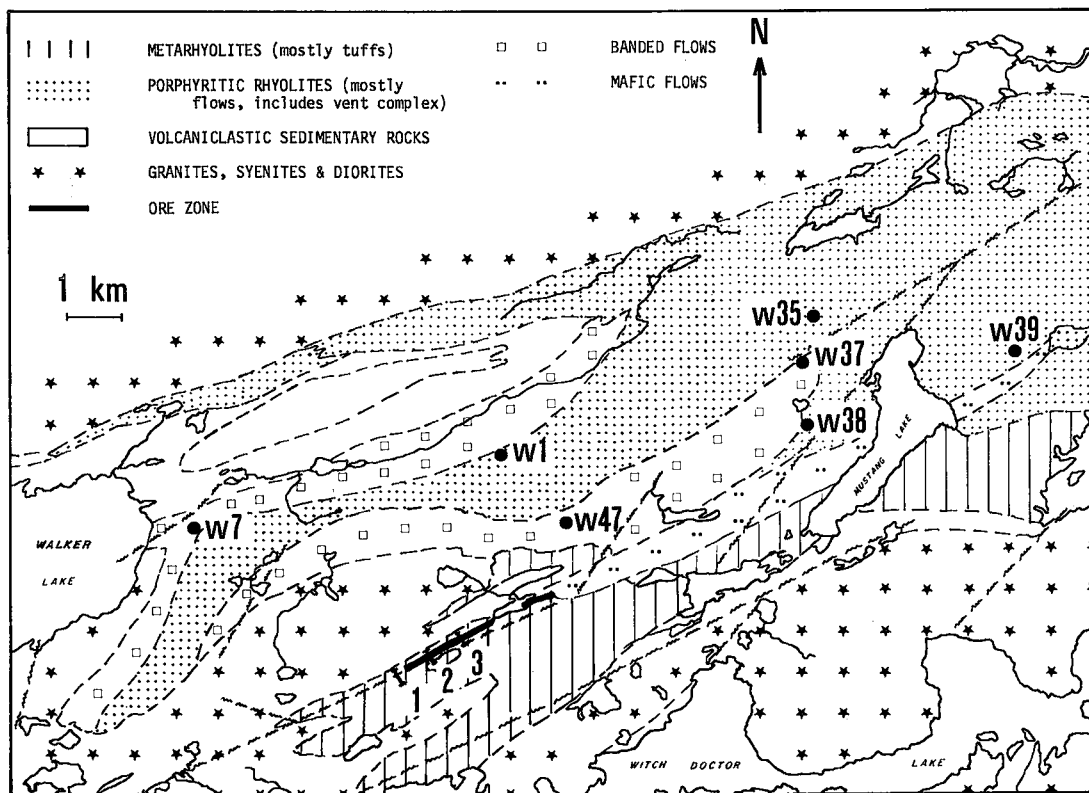


FIG. 1. Simplified geological map of the Michelin area showing the location of all but two specimens used in this study (● individual specimens, I composite samples). The map, adapted from the base map of Watson-White (1976), was updated slightly in view of recent geological mapping by the Government of Newfoundland and Labrador (especially that of D.G. Bailey) and by British Newfoundland Exploration Limited (Brinex). The average bulk composition of the three composite samples is listed in Table 5: (1) nonmineralized ignimbrite, cross-section M31 ( $n = 34$ ); (2) mineralized tuffs away from the ore zone and (3) "Or" series of specimens from the ore zone (1, 2 and 3 sampled from drill core).

Our aim in this paper is to present textural, mineralogical and compositional information bearing on (1) the nature of the primary volcanic assemblage and (2) the metasomatic events that accompanied uranium mineralization in the pyroclastic and shallow intrusive units of the Upper Aillik Group. We avoided rocks that appeared to have undergone strong recrystallization during subsequent orogenies; also, we focused our attention on the Michelin – Burnt Lake belt of mineralization and on the shallow intrusive rhyolite body at White Bear Mountain, approximately 30 km along strike to the northeast [see Gandhi (1978) for geographical locations and a compilation of the regional geology].

#### GEOLOGICAL SETTING OF THE MICHELIN – BURNT LAKE – WHITE BEAR MOUNTAIN BELT

The Aillik Group consists of a lower division of metamorphosed pillowed basic volcanic and sedimentary rocks and an upper division in which felsic volcanic rocks predominate over conglomerates and minor intercalated basic volcanic flows (Smyth 1977). The deformed felsic volcanic sequence of the upper division consists largely of ignimbrites, pyroclastic deposits in which fragments of vesiculating juvenile material (pumice fragments, glass shards) formed a dominant component (Sparks *et al.* 1973); of local importance are porphyritic rhyolite domes and minor agglomeratic and tuffaceous deposits. Prominent lithologies in the upper portion of the Aillik Group are feldspar and quartz–feldspar porphyritic rhyolite ash-flow tuff (welded and nonwelded), minor nonporphyritic rhyolite ash-flow tuff, minor tuffaceous sandstone and siltstone, and minor basic flows and tuffs (Bailey 1978). Bailey also noted that the nonporphyritic ash-flow tuffs commonly grade into bedded ash-fall tuffs. A simplified geological map of the area of interest (Fig. 1) shows the location of the ore zone and of most of the specimens on which this study is based. The uranium occurrences in this belt are also shown by Gandhi (1978, Fig. 13). We also sampled a domal subvolcanic complex of comagmatic porphyritic rhyolite at White Bear Mountain (specimens W49a, W49b, W50), mapped by Bailey *et al.* (1979) but beyond the area of Figure 1 to the northeast. The economic concentrations of uranium occur mainly in shear zones in rhyolitic tuffs. Evans (1980) and Gandhi (1978) have proposed that uranium was precipitated on sphene and with Fe–Ti–Mn oxides, including members of the

davidite family (Minatidis 1976), in environments of chemical reduction.

#### TEXTURES IN THE RHYOLITES

Deformation associated with the Hudsonian orogeny has largely obliterated most primary textures in the tuffs and porphyries; only locally can textural features be compared with those encountered in young ignimbrites. For example, Clark (1971) identified relict euhedral quartz grains in his “porphyroclastic psammite”. We interpret the rhombic and hexagonal cross-section illustrated by Clark as indicating that these grains, now  $\alpha$ -quartz, are paramorphic after  $\beta$ -quartz phenocrysts. Clark’s illustrations document well the partial obliteration of this textural information as a result of postdeformation recrystallization of single crystals into monomineralic aggregates, presumably to eliminate strain. Only locally can subhedral and amoeboid grain shapes expected of the rapid growth of  $\beta$ -quartz be found unaffected (Fig. 2).

Even more susceptible to obliteration than the diagnostic shape of  $\beta$ -quartz phenocrysts are the eutaxitic and spherulitic textures in the fine-grained matrix material of the tuffaceous felsic rocks. Watson-White (1976) has found Upper Aillik Group rocks with such textures in the Michelin-Walker Lake-Mustang Lake area (Gandhi 1978); these are much less thoroughly deformed than analogous units near Kaipokok

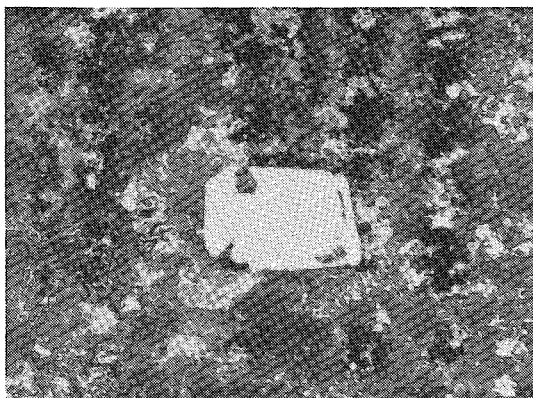


FIG. 2. Amoeboid, subhedral quartz phenocryst (1 mm across) with granophyric fringe in rhyolite porphyry W49a. Such skeletal crystals are paramorphic after  $\beta$ -quartz and do not reflect episodes of magmatic corrosion. Sampled from the plug that forms White Bear Mountain (not shown in Fig. 1).

Bay (Clark 1971, 1979, Marten 1977). In drill core from the Michelin deposit, delicately laminated rhyolite occurs in association with thin basic flows and more coarsely banded and massive rhyolitic units. Deformation commonly seems to have accentuated an original planar fabric in the tuffs; metamorphic minerals define the fabric: chlorite, epidote and biotite in felsic units, epidote and actinolite in mafic bands. The same minerals define fabrics in the more deformed rocks to the northeast (Clark 1979).

The well-banded rhyolites that flank Michelin Ridge and that occur between Mustang and Walker lakes (unit 4b of Bailey 1978) are pinkish to grey, fine-grained to aphanitic; they generally contain no visible crystal fragments. In thin section, sparse, broken crystal fragments and abundant elongate lithic fragments commonly show signs of rotation. The slightly coarser-grained quartzofeldspathic lenses in these rocks are carbonate-bearing; that they are bent and in some cases folded may indicate that the lenses were pumice fragments, deformed during flattening. Some of these banded rhyolites are recrystallized ignimbrites, whereas in others, the prominent banding may well be a result of flow in felsic lavas. The aphanitic matrix, generally showing granoblastic equant to lenticular grains of quartz and two feldspars (rarely visibly twinned), locally still is spherulitic to axiolitic, though these textures also show signs of recrystallization, coarsening and deformation dur-

ing later movement (Fig. 3). Here, the spherulitic texture most probably indicates devitrification of glassy material, with coarsening by annealing prior to deformation.

The devitrified porphyritic obsidians and rhyolites commonly contain areas of granophyric texture developed as fronds of intergrown quartz and alkali feldspar that mantle amoeboid, skeletal quartz (Fig. 2) and feldspar phenocrysts. Interestingly, the aphanitic rocks sampled near the edge of a rhyolite plug at White Bear Mountain, which show "cellular" (Fig. 4) and modified spherulitic textures, grade laterally into rhyolites, showing granophyric mantles on phenocrysts and granophyric inclusions within phenocrysts. These examples of granophyric intergrowths probably developed by rapid crystal growth from liquid immediately following growth of the phenocrysts, and thus at the magmatic stage, in response to sudden cooling or gas-phase escape (or both) during emplacement of the rhyolite dome. Near the contacts, the groundmass must have been largely glassy. As in the case of the banded rhyolites, the spherulitic textures in these shallow intrusive rocks can be interpreted as a devitrification phenomenon, catalyzed by the influx of aqueous fluids (Lofgren 1970, 1971).

In some rocks, the granophyric intergrowth does not consist of the customary short vermicules of quartz and feldspar but of alternating tablets or rods of the two minerals (Fig. 5). These also occur in trapped melt inclusions with-

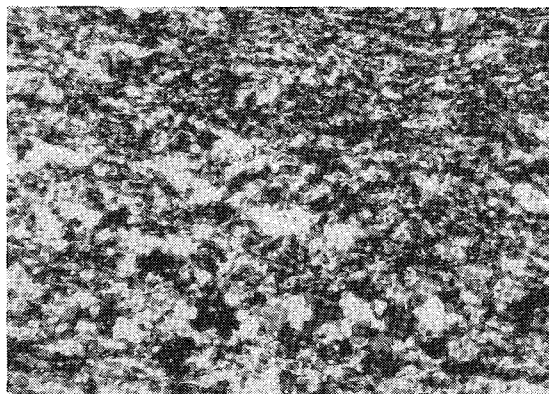


FIG. 3. Lenticular and axiolitic components of rhyolitic tuff W37, of probable ash-flow origin. The tuff also contains lenticular brownish lithic inclusions and pink, fine-grained bands that show signs of incipient recrystallization to a granoblastic texture. Same scale as Figure 2.



FIG. 4. Cellular and modified spherulitic texture in porphyritic rhyolite W49b, sampled near the edge of the intrusive rhyolite plug at White Bear Mountain. The perthite phenocryst is texturally disturbed but probably close to original bulk composition. W49b grades laterally into W49a (Fig. 2).

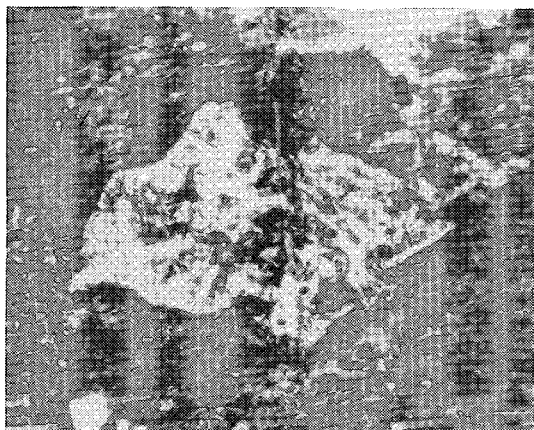


FIG. 5. Trapped melt inclusion in alkali feldspar phenocryst in porphyritic rhyolite W35. The tablets (now quartz) are interpreted to have been tridymite, an indication of final crystallization at high temperatures ( $>900^{\circ}\text{C}$ ) at or near the surface. The field of view is 0.7 mm across.



FIG. 6. Overgrowth of sanidine (now coarse, blotchy microcline perthite) around albitized, calcite-speckled anhedra plagioclase core. These phenocrysts have not retained their original bulk composition. Same porphyritic rhyolite as in Figure 2; field of view is 3.3 mm across.

in phenocrysts. Such distinctive intergrowths, described from Skaergaard by Wager *et al.* (1953), from Sudbury by Stevenson (1963) and from the Muskox intrusion by Pouliot (1968), have been interpreted as tridymite-alkali feldspar intergrowths, with tridymite tablets now inverted to polycrystalline aggregates of  $\alpha$ -quartz. That such an assemblage forms in the groundmass and occurs within phenocrysts in a rhyolitic magma in which  $\beta$ -quartz phenocrysts nucleated confirms the high-temperature origin of the granophyric texture and its appearance at higher crustal levels (lower confining pressure) than the phenocryst phase. The field of stability of tridymite is relegated to a high temperature and low pressure: above  $867^{\circ}\text{C}$  at 1 atm,  $1000^{\circ}\text{C}$  at 750 bars.

#### TEXTURES IN THE FELDSPAR PHENOCRYSTS

It is in phenocrysts in the porphyritic rhyolites that the feldspars most closely approach, texturally at least, their primary character. The feldspar phenocrysts, generally more prominent than the paramorphs after  $\beta$ -quartz phenocrysts, are euhedral, subtly zoned and perthitic. In several instances, the feldspar grains are in fact composite, consisting of a mantle of alkali feldspar on an irregularly shaped core of sodic plagioclase (Fig. 6). In other cases, the anhedra plagioclase is only partly mantled, a feature that probably indicates the breakup of the composite phenocrysts during emplacement. The

polysynthetic twins in the sodic plagioclase cores, usually wavy owing to later deformation, typically extend across the entire crystal, in contrast to the chessboard albite domains in the perthite rims (Fig. 7). The plagioclase cores cannot be truly xenocrystic, because they too contain irregular tridymite-bearing granophyric inclusions, as found in the alkali feldspar and quartz phenocrysts. If our interpretation of these as inclusions of trapped melt is correct, the sodic plagioclase must form part of the crystallization sequence of the rhyolites. The sequence of primary crystallization thus seems to have been plagioclase  $\rightarrow$  alkali feldspar (in cases concentrically zoned)  $\rightarrow$   $\beta$ -quartz  $\rightarrow$  tridymite + sanidine (inferred) in the groundmass and in melt inclusions.

It is also interesting to record the textural aspect of the perthitic intergrowths. In the most pristine rhyolites, the perthite consists of a regular, braid-like alternation of albitic lamellae and slightly dusty K-feldspar. The proportion of these two is relatively constant across the euhedral phenocryst except where there is primary concentric zoning, generally most evident near the edge of crystals. The regularity of the two-phase array is interpreted ultimately to be a result of exsolution, though the scale of the intergrowth (Fig. 8) is coarse for phenocrysts in a volcanic rock. The width of the lamellae, the sharpness of the interface between domains and the development of the grid pattern typical of microcline in the K-feldspar host rule out the possibility that these phenocrysts contain co-

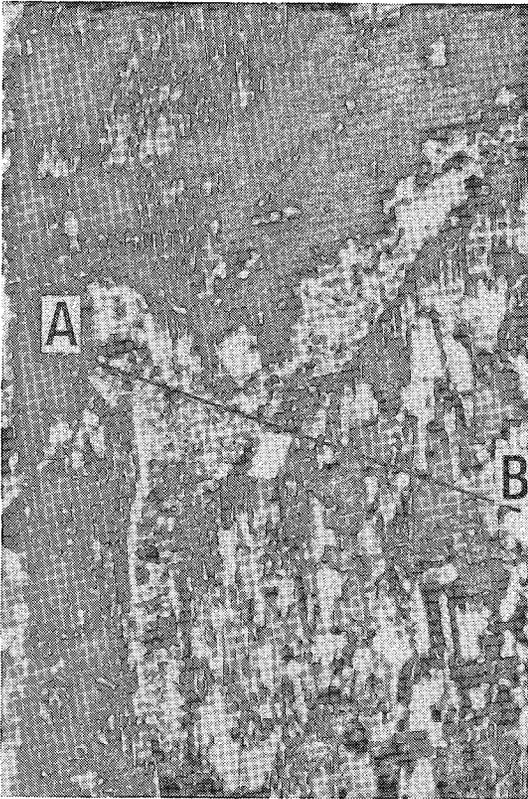


FIG. 7. Outer portion of a composite phenocryst such as shown in Figure 6. This one, found in porphyritic rhyolite W35, shows a sliver of K-rich quartz-bearing matrix along the left edge of the photograph, a dark two-phase rim at A in which  $K > Na$ , an inclusion of devitrified melt such as shown in Figure 5 (also from W35) in which  $K \gg Na$ , an outer core of chessboard albite in which  $Na > K$ , and an inner core of albitized plagioclase [not shown (to the right of B) but similar to that in Figure 6]. Note the calcite rhomb midway along the microprobe traverse from A to B.

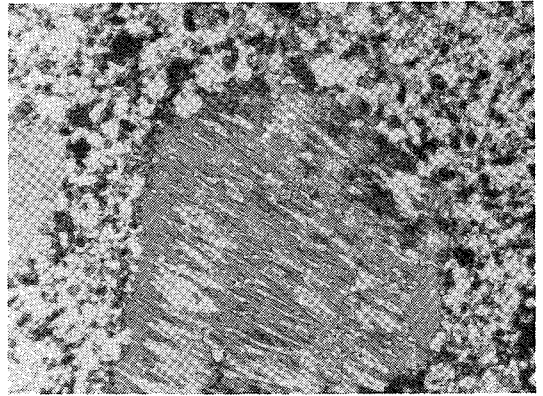


FIG. 8. Texturally disturbed perthite in porphyritic rhyolite W50, sampled at White Bear Mountain near the contact with a younger gabbro plug (not shown in Fig. 1). The original bulk composition may not have been affected seriously except at the edges of the grain. Field of view is 3.3 mm across.

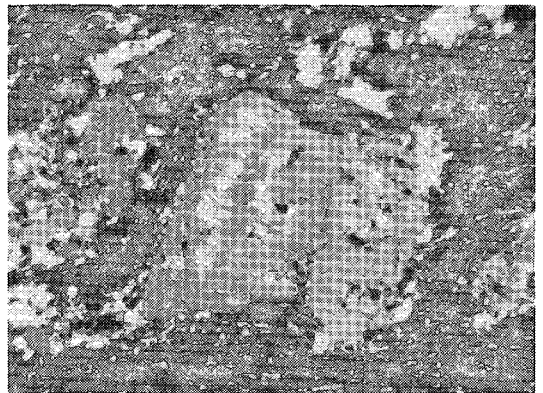


FIG. 9. Almost completely K-metasomatized perthite fragment in banded rhyolitic tuff W1. Albite remains in islands away from the grain edges; the bulk of the fragment is dusty microcline. No albite remains in the matrix. Field of view is 3.3 mm across.

herent intergrowths of the two feldspars. Rather, the perthitic intergrowths have been texturally modified by coarsening during deuteric recrystallization and perhaps also as a result of subsequent deformation and local contact metamorphic effects surrounding the postorogenic intrusions.

More typical of the feldspar phenocrysts encountered in the porphyritic rhyolites are microcline-albite intergrowths in which the two phases occupy very irregular patches (Figs. 8, 9). The microcline typically shows the character-

istic cross-hatched pattern, whereas the albite is a chessboard array of irregular, discontinuous albite-twinned domains. In our opinion, these patterns of distribution of sodic and potassic domains represent modified exsolution-perthite textures. The modification has involved short-range migration and coarsening of domains (Fig. 8), without serious disturbance of overall bulk compositions; proportions of K- and Na-feldspars are subequal. However, the same can-

not be said about the broken phenocrysts in tuffaceous rocks; in many cases, these grains may now be monomineralic, either all (or almost all) microcline (Fig. 9), in narrow elongate domains giving a heterogeneous, mottled appearance, or all chessboard albite. In some such crystals, vestiges of the original Carlsbad twin boundary can still be seen.

The fine-grained groundmass feldspars in the porphyritic rhyolites and in the tuffs are also of real interest, because they invariably reflect more sensitively the compositional changes that may be incipiently developed only in the coarser grains. Only rarely, however, are there visible signs that compositional changes have occurred; the fine grains are generally homogeneous, anhedral (granoblastic) and free of internal structures. One must resort to comparative studies of structural and compositional variables by X-ray-diffraction techniques.

STRUCTURAL STATES AND COMPOSITIONS OF THE FELDSPARS

Phenocrysts and adjacent groundmass have been studied in detail to obtain information on (1) compositions (2) structural states and (3) proportions of coexisting phases. The electron microprobe was used to obtain point analyses in certain phenocrysts showing patterns of patchy extinction. Detailed X-ray-diffraction studies of very small samples (Guinier-Hägg focusing camera, Cu K $\alpha_1$  radiation, synthetic spinel internal standard) provided the rest of the information.

The phenocryst shown in Figure 7, from porphyritic rhyolite W35, is surrounded by a potassium-rich quartz-bearing matrix that contains specks of calcite. A probe traverse across the grain first encounters a K-rich two-phase rim (A in Fig. 7) in which the distribution of microcline (darker, predominant) and chessboard albite is clearly patchy. The irregular, sharply delimited, light-colored film of granophyric tridymite + sanidine (now inverted), here interpreted as trapped melt inside the phenocryst, is very rich in K and correspondingly poor in sodium. The next zone can be described as an outer core of chessboard albite; it is generally K-poor, although small K-rich domains do occur along the probe traverse. The inner core (Fig. 6; to the right of B, not shown in Fig. 7) consists of albite-twinned sodic plagioclase, an area free of K-feldspar domains. The abundance of calcite specks in this core area suggests that the pure albite there is not primary, and that the plagioclase may have been oligoclase

TABLE 2. COMPOSITION AND DEGREE OF Si-Al ORDER OF ALBITES AND MICROCLINES, AS INFERRED FROM CELL-DIMENSION DATA

Specimen	$\Delta$	$\psi$	$\Delta\alpha^{**}$	$\Delta\delta\alpha$	$\Delta\epsilon$	$\Delta\zeta$	#
313	-0.015	0.994	0.993	0.993			1.084
315	-0.020	0.988	1.006	0.997			1.097
350a	-0.027	0.981	0.968	0.974			1.154
Or80	-0.017	0.983	0.987	0.985			1.111
Or81	-0.017	0.981	0.994	0.988			1.105
Or82	-0.015	0.974	0.988	0.981			1.110
Or83	-0.020	0.978	0.985	0.982			1.095
Or84	-0.020	0.981	0.980	0.981			1.109
W37 pink matrix	0.966	0.988	1.018	1.003	0.983		1.102
W37 brown matrix	0.968	1.003	1.021	1.012	0.986		1.110
W47 grey matrix	0.964	1.010	1.005	1.008	0.996		1.136
W47 pink matrix	0.972	0.995	1.035	1.015	1.005		1.121
W1 phenocryst	0.961	1.010	1.009	1.010	0.986		1.096
W1 matrix	0.964	1.001	0.997	0.999	0.961		1.091
W35 phenocryst	1.006	1.006	1.006	1.006	0.958		1.078
W35 matrix	0.955	0.991	1.009	1.000	0.977		1.129
W38 phenocryst	0.952	0.997	1.032	1.014	1.047		1.129
W38 matrix	0.966	0.967	1.027	1.007	0.985		1.129
W39	-0.012	0.979	0.970	0.975			0.927
W49b phenocryst	0.946	1.006	0.991	0.999	0.927		1.143
W49b matrix	0.950	0.989	1.019	1.004	0.980		1.125
W50 phenocryst	0.965	0.999	1.020	1.010	0.996		1.099
W50 matrix	0.989	0.992	1.021	1.006	0.941		1.110
W49a phenocryst	0.944	0.978	0.978	0.978	0.978		1.197
W49a grey matrix	0.959	0.972	0.929	0.950	0.920		1.166
W49a pink matrix	0.942	0.946	0.978	0.962	0.979		1.151
W7	0.983	1.009	1.014	1.012	0.988		67

$\Delta$  or  $\psi$  is calculated from unit-cell volume by the expression of Stewart & Wright (1974); albites commonly give negative values with this expression. Values of  $\Delta\epsilon_1 + \Delta\epsilon_{2m}$  (i.e.,  $\Delta\epsilon$  in  $Z_1O + Z_{2m}$  sites, =  $\Delta\delta\alpha$ ) and  $\Delta\zeta_1 - \Delta\zeta_m$  (=  $\Delta\alpha^{**}$ ) are obtained using the expressions of Blasi (1977). Calculated standard errors are  $\pm 0.0069$  and  $\pm 0.0063$ , respectively, on the average. Values of these indices should not exceed 1.000, yet in many microclines in this suite, (1)  $\Delta\delta\alpha > 1$  and (2)  $\Delta\alpha^{**} > \Delta\delta\alpha$  (see text). For microclines,  $\Delta$  is obliquity,  $12.5(\Delta_{131} - \Delta_{131})$ ; for albites,  $\psi = 2\theta_{131} - 2\theta_{31}$ . Both  $\Delta$  and  $\psi$  are calculated values. # refers to the number of indexed peaks on which the cell refinement (program of Appleman & Evans 1973) is based (see Table 1). Specimens W35, W38, W49a, W49b and W50 are porphyritic rhyolites; the rest is a collection of rhyolitic tuffs. Among these, specimens 313 and 315 were taken from drill core in cross-section 2 (Fig. 1), 350a is from cross-section 1 and Or80  $\rightarrow$  Or84, from cross-section 3 (Fig. 1).

or andesine. A map of the distribution of Na and K for this mantled grain and microprobe analyses of other grains substantiate the findings outlined above: fine-grained material, such as the matrix and granophyric inclusions may be strongly disturbed compositionally, being highly enriched in K in W35, whereas coarser grains of alkali feldspar are more likely to contain microcline and albite in proportions that seem original (i.e., subequal), especially away from grain margins.

The a cell dimension and the unit-cell volume calculated from carefully indexed powder patterns (cell dimensions in Table 1, available from the Depository of Unpublished Data, CISTI, The National Research Council of Canada,

Ottawa, Ontario K1A 0S2 and from the authors) provide compositions that support the results obtained by microprobe.

Compositions expressed in terms of  $N_{or}$  (pure  $KAlSi_3O_8 = 1.0$ ) are tabulated for phenocrysts and adjacent groundmass in five porphyritic rhyolites and three banded rhyolitic tuffs (Table 2); also tabulated are data for one dyke rock in banded rhyolite and for nine laminated felsic rocks, eight of which are sampled from drill core at the Michelin deposit. All alkali feldspar assemblages encountered consist of pure albite ( $-0.027 < N_{or} < -0.007$  based on unit-cell volume: Table 2) and essentially pure microcline ( $0.942 < N_{or} < 1.006$ ). The purity of these coexisting alkali feldspars indicates equilibration temperatures down to  $200^\circ\text{C}$  (e.g., Smith 1974, Fig. S-1, Bachinski & Müller 1971, Fig. 9).

An interesting question that can be solved by the collected X-ray-diffraction data concerns the proportion of the K-rich and Na-rich feldspars in each fraction sampled. As both feld-

spars have triclinic cells and share a common structure, the number of planes along which they diffract X-rays is approximately the same. The ratio of diffraction lines unambiguously assigned to the K-feldspar to the total number of assigned lines thus gives a rough indication of the volume of K-feldspar present. In the angular interval considered ( $13-65^\circ 2\theta$ ), the total number of feldspar peaks read and indexed typically ranges from 60 to 70 for two-feldspar assemblages. Of this number, between  $\frac{1}{3}$  and  $\frac{2}{3}$  of the peaks is assigned to K-feldspar in the alkali feldspar phenocrysts of five porphyritic rhyolites (Fig. 10). This variation in bulk composition could be largely primary and only mildly affected by the recrystallization that has led to the coarsening of the exsolution perthite structure. Note that the feldspar assemblage recorded in the groundmasses converges to a value of 40% K-feldspar in four of the five rhyolites. The similarity between this value and the bulk feldspar composition expected during the final stages of low-pressure crystallization of a haplogranitic liquid (Tuttle & Bowen 1958, Fig. 23) is striking, considering the low accuracy of such an evaluation of bulk composition of the feldspar assemblage. We contend that porphyritic rhyolite W38, whose groundmass apparently contains more than 50% K-feldspar, shows the effects of mild K-metasomatism. In specimen W49a, the grey matrix represents the more pristine composition; the pink streaks, which seem to accentuate flow layering, are marginally richer in albite and may indicate the effects of incipient or mild Na-metasomatism along zones of enhanced permeability.

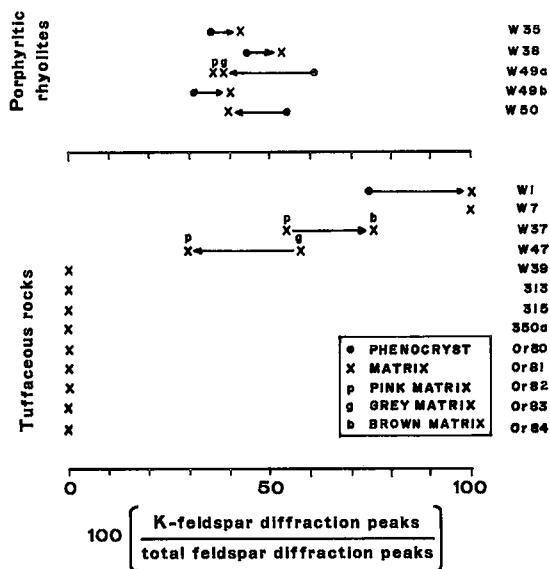


FIG. 10. Approximate bulk composition of alkali feldspar assemblages, estimated by the proportion of observed diffraction peaks identified as belonging to K-feldspar (for inherent assumptions, see text). This information is shown for phenocryst (●) and matrix (x); where different colors of matrix were observed, these were sampled separately [labeled p (pink), g (grey) or b (brown)]. Note that compositional disturbances are most profound in tuffaceous rocks.

In contrast to the porphyritic rhyolites, the tuffaceous rocks show clear effects of strong alkali metasomatism. Rock W1 is so strongly K-metasomatized that the groundmass contains only microcline + quartz, and no albite; the fragments of perthite also show marked K-enrichment over any phenocryst found in the porphyritic rhyolites. The same applies to dyke rock W7. All eleven other tuffaceous rocks show the effects of strong Na-metasomatism, leading, in extreme cases found in and near the ore zone at Michelin, to rocks containing albite + quartz or albite alone (see next section). In W47, a very fine-grained rock free of obvious feldspar crystal fragments, the predominant dark grey portion of the rock does not contain as much albite as do the pink streaks developed around lithic fragments and along cracks (Fig. 10). The much stronger effects of K- or Na-metasomatism in the tuffs is undoubtedly largely a function of

(1) their permeability and (2) the large surface area of the feldspar grains with respect to their volume. Using bulk chemical compositions, Watson-White (1976), Gandhi (1978) and Evans (1980) noted the importance of sodium metasomatism in the mineralized tuffs of the Michelin deposit.

#### Degree of Si-Al order of the feldspars

The cell dimensions of the feldspars also provide an indirect measurement of the degree of Si-Al order. The values of  $t_1O$ , the Al occupancy of the  $T_1O$  site in the feldspar structure, can be calculated from the  $b$ ,  $c$ ,  $\alpha^*$  and  $\gamma^*$  cell dimensions (Stewart & Ribbe 1969, Blasi 1977).

All the rocks studied contain well-ordered albite, microcline, or both. In the tuffs, many microclines encountered are "anomalously" well ordered, as values of  $t_1O$  exceed 1.0 (attaining 1.015); the maximum is set at 1.0 by definition. Such values, exceeding the upper limit and also noted in many microclines from the porphyritic rhyolites, have been found characteristic of moderate-temperature feldspars formed in peralkaline environments (Martin 1977, Siemiatkowska & Martin 1975). The peralkalinity of the aqueous fluid that catalyzed the Si-Al ordering reactions is probably reflected in the resulting microcline, because the dissolution steps necessary for ordering are much more efficient in high-pH media (Martin 1974). One might expect that such rates of conversion would be greater in the tuffs than in the less permeable rhyolites, and greater in the groundmass than in the phenocrysts. Plots of  $b$  versus  $c$  and  $\alpha^*$  versus  $\gamma^*$  on which lines are drawn between coexisting Na- and K-feldspars show clearly that the degree of Si-Al order in feldspars from tuffs is generally greater than in some porphyritic rhyolites, and that the best-ordered feldspars (largest  $c$  and  $\gamma^*$ ) are to be found in the tuffs.

Interestingly, the sodic plagioclases in the porphyritic rhyolites and tuffs seem not quite as well ordered as the microclines: values of  $t_1O$  range from 0.936 to 0.997 (Table 2), and no anomalous values exceeding 1.0 are encountered. Two factors must be considered in searching for an explanation of calculated values of  $t_1O$  that fall significantly short of 1.0: (1) slight departures from perfect long-range order, and (2) small amounts of calcium in the structure which, because of coupled Al-for-Si substitution, affect the cell parameters in a similar fashion.

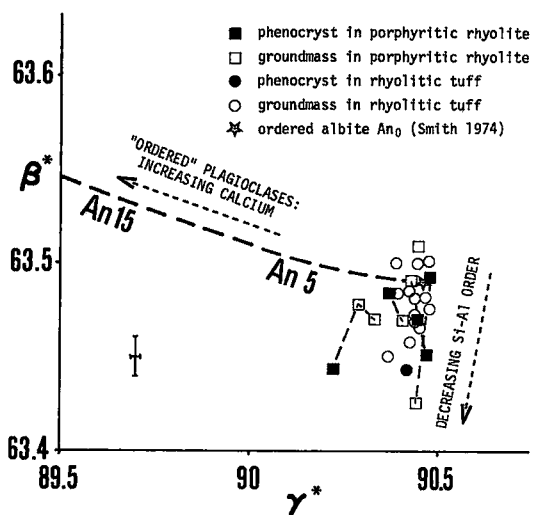


FIG. 11. Plot of  $\beta^*$  versus  $\gamma^*$  for the sodic plagioclases encountered in the porphyritic rhyolite and rhyolitic tuff specimens. Representative error bars ( $\pm 1\sigma$ ) are presented in the lower left-hand corner.

Smith (1974, Fig. 7-44) found the  $\beta^*$ - $\gamma^*$  plot particularly appropriate to resolve the ambiguity between the composition and structural state of plagioclases. In a plot of  $\beta^*$ - $\gamma^*$  values, the 16 albites associated with microclines in porphyritic rhyolites and some tuffs and the 9 albites found as the major constituent of strongly albitized tuffs cluster closely about the point for fully ordered, calcium-free albite (Fig. 11). Some data plot below this point, along a trend normal to the direction of increasing An content; these albites probably also are calcium-free but depart slightly from complete long-range Si-Al order. Martin (1974) has proposed that such slight departures may result from the Na-metasomatism of oligoclase or andesine. The anhedral sodic plagioclase cores peppered with calcite specks (Fig. 6) thus seem to be pseudomorphs of oligoclase or andesine. Coordinates for three data points for rock W49a, which depart the most from the  $An_0$  isopleth, suggest slightly disordered  $An_{3-4}$ , presumably the result of arrested Na-metasomatism of oligoclase or andesine.

#### WHOLE-ROCK GEOCHEMISTRY

##### Major elements

Whole-rock analyses of selected specimens of

TABLE 3. BULK COMPOSITIONS OF PORPHYRITIC RHYOLITES AND RHYOLITIC TUFFS, AILLIK GROUP

	313	315	350a	Or80	Or81	Or82	Or83	Or84	W37	W47	W1	W35	W38	W39	W49b	W50	W49a	W7
SiO <sub>2</sub>	69.90	76.40	75.14	64.00	70.10	65.90	65.20	64.10	77.46	76.81	72.90	74.35	77.29	71.71	72.95	71.51	70.94	65.37
TiO <sub>2</sub>	0.37	0.24	0.34	0.84	0.50	0.34	0.44	0.67	0.11	0.13	0.29	0.37	0.18	0.32	0.42	0.44	0.39	0.15
Al <sub>2</sub> O <sub>3</sub>	11.50	11.90	12.55	16.00	13.30	16.90	17.10	17.00	11.30	11.82	12.83	12.30	11.18	14.57	13.39	13.34	14.40	17.35
Fe <sub>2</sub> O <sub>3</sub>	1.79	1.43	1.80	3.07	2.97	2.92	2.21	2.12	0.78	0.90	1.45	1.92	1.04	2.22	1.30	2.11	1.52	1.51
FeO	1.61	1.29	1.62	2.77	2.68	2.63	1.99	1.91	0.71	0.81	1.31	1.73	0.94	2.00	1.17	1.90	1.37	1.36
MnO	0.11	0.04	0.05	0.06	0.08	0.07	0.07	0.14	0.02	0.01	0.03	0.04	0.01	0.02	0.06	0.11	0.05	0.02
MgO	0.69	0.13	0.24	0.46	0.26	0.13	0.29	0.83	0.01	0.00	0.00	0.00	0.03	0.24	0.15	0.35	0.19	
CaO	7.82	1.07	1.22	1.81	1.05	3.00	1.90	2.92	0.26	0.42	0.37	0.58	0.23	0.82	0.62	0.72	1.37	1.14
Na <sub>2</sub> O	6.29	7.54	6.76	11.00	8.51	8.30	10.80	10.50	1.18	2.34	0.71	4.02	2.01	8.04	4.37	4.18	4.14	0.52
K <sub>2</sub> O	0.13	0.06	0.42	0.14	0.09	0.15	0.08	0.10	8.24	6.84	10.23	4.85	7.21	0.47	5.59	5.72	5.59	12.53
P <sub>2</sub> O <sub>5</sub>	0.05	0.03	0.04	0.09	0.06	0.02	0.12	0.14	0.01	0.01	0.03	0.04	0.01	0.02	0.03	0.03	0.05	0.03
F	0.06	0.03	0.03	0.03	0.02	0.03	0.02	0.05	0.02	0.02	0.02	0.01	0.02	0.03	0.14	0.05	0.10	0.03
Cl	0.01	0.01	0.00	0.01	0.01	0.02	0.01	0.00	0.00	0.01	0.00	0.00	0.00	0.01	0.00	0.01	0.01	0.00
S	0.07	0.09	0.23	0.07	0.10	0.04	0.06	0.03	0.00	0.00	0.00	0.00	0.00	0.00	0.00	0.00	0.00	0.02
CO <sub>2</sub>	2.32	0.45	0.02	0.15	0.10	0.30	0.75	1.10	0.15	0.02	0.15	0.40	0.10	0.25	0.05	0.05	0.05	0.02
ZrO <sub>2</sub>	0.04	0.05	0.06	0.12	0.14	0.00	0.10	0.20	0.02	0.03	0.04	0.06	0.03	0.07	0.06	0.09	0.04	0.03
Σ	102.76	100.76	100.52	100.62	99.97	100.75	101.14	101.81	100.27	100.17	100.36	100.67	100.25	100.58	100.39	100.41	100.34	100.25
U	79.2	16	130	3700	530	1180	1550	3000	8	9	4	3	2.6	7.3	11	4.3	8.9	11
Th	12	30	27	22	37	16	9	31	32	29	28	22	17	13	28	18	20	44
Pb	30	30	30	1230	330	160	400	930	20	20	60	0	20	30	20	70	80	70
Zn	90	80	50	48	200	28	54	19	40	40	20	20	40	290	90	150	60	90
Cu	30	30	30	2	1	3	4	3	20	20	0	50	20	230	40	50	30	10
D.I.	79.6	92.9	91.5	81.4	87.2	82.5	88.7	87.5	97.4	96.2	95.5	94.6	97.2	92.3	95.1	92.9	90.5	89.8
A.I.	0.91	1.05	0.92	1.14	1.06	0.82	1.04	1.02	0.96	0.95	0.95	0.96	0.99	0.94	0.99	0.98	0.89	0.83
Ab	66.7	65.5	62.5	99.0	77.9	85.0	98.6	99.3	10.3	20.5	6.3	36.0	17.5	73.6	38.9	38.0	38.6	4.9
Or	1.0	0.4	2.7	1.0	0.6	1.1	0.5	0.7	50.0	42.0	63.3	30.3	43.8	3.0	34.7	36.4	36.5	82.5
Q	32.3	34.1	34.8	0	21.5	14.0	0.8	0	39.8	37.5	30.4	33.7	38.7	23.4	26.4	25.6	24.9	12.7

Analyses by X-ray-fluorescence techniques (except U and Th, determined by delayed neutron activation). D.I. is the sum of normative orthoclase (Or), albite (Ab), quartz (Q) and nepheline (Ne). A.I. is the agpaite index, the molar ratio  $(Na_2O+K_2O)/Al_2O_3$ . Specimens 313, 315, and 350a are finely laminated rhyolitic tuffs, Or80, Or81, Or82, Or83 and Or84 are laminated tuffs from the ore zone at Michelin, W37, W47 and W1 are banded rhyolitic tuffs, W35 and W38 are porphyritic rhyolites, W39 is a laminated rhyolitic tuff, W49b and W50 are porphyritic rhyolites, W49a is a rhyolite porphyry and W7 is a microcrystalline dyke rock emplaced in finely banded rhyolite 0.75 km E of Walker Lake. Ten replicate XRF analyses of one specimen were done to evaluate analytical errors. These are quoted as a ± value (in %) of the amount present: SiO<sub>2</sub> 1.2, Al<sub>2</sub>O<sub>3</sub> 1.6, K<sub>2</sub>O 2.4, total Fe expressed as Fe<sub>2</sub>O<sub>3</sub> 2.6, Na<sub>2</sub>O 6.3, CaO 10, TiO<sub>2</sub>, P<sub>2</sub>O<sub>5</sub> 20, MgO 27. The high standard errors reflect the very low levels of Ca, Ti, P and Mg (typical of nonorogenic felsic rocks) rather than a poor analytical technique.

rhyolites and tuffs have been obtained by X-ray-fluorescence techniques (Table 3). These analyses complement the bulk-composition data obtained by Gandhi (1978). The 31 sets of data available are represented in terms of normative Q–Ab–Or (Fig. 12) and the molar proportions (Na+K)–Al–Si (Fig. 13). The rocks range in the differentiation index (D.I.:  $\Sigma Q + Ab + Or$  in the norm) from 78 to 97; the average D.I. is 89. They vary in composition from ultrasodic to ultrapotassic, the extremes invariably being very fine grained. The seven rocks in the central portion of Figure 12 probably are very close to their original bulk composition; among the seven are rocks selected to illustrate the least-disturbed textural features. Note that the Na-metasomatized tuffs in the ore zone at Michelin define a range in normative quartz content from 44% down to nil. We propose that the specimen of tuff that contains 44% quartz was hydrothermally silicified, because the pristine rocks contain less than 35% normative quartz. The sodic tuffs that contain between 25 and 35% normative quartz probably have evolved by Na-

for-K exchange imposed on "centrally located" rocks in Figure 12. Such ion-exchange reactions are rapid, as they involve no change in Al/Si ratio. The mildly metasomatized bulk compositions give way to silica-depleted rock types, leading to albitites in the extreme cases. As no fresh trachytes have been found in the Michelin area, we contend that these albitite tuffs have evolved by strong (Na + Al)-metasomatism rather than by simple ion-exchange. The efficient desilication involved is characteristic of countless cases of fenitization, in which high-pH aqueous fluids interact with rocks of more normal alkalinity. We are dealing here with a case of autometasomatism, in which late-stage alkaline fluids have removed quartz of primary origin.

The agpaite index (Na + K)/Al of these rocks ranges from 0.818 to 1.468 (average 1.015). Most of the pristine, quartz-bearing specimens have agpaite indices close to 1; they range from slightly subalkaline to mildly peralkaline. The role of a peralkaline fluid medium in the desilication of the tuffs is confirmed, as the quartz-poor bulk compositions are all peralkaline (Fig. 13). This confirms the

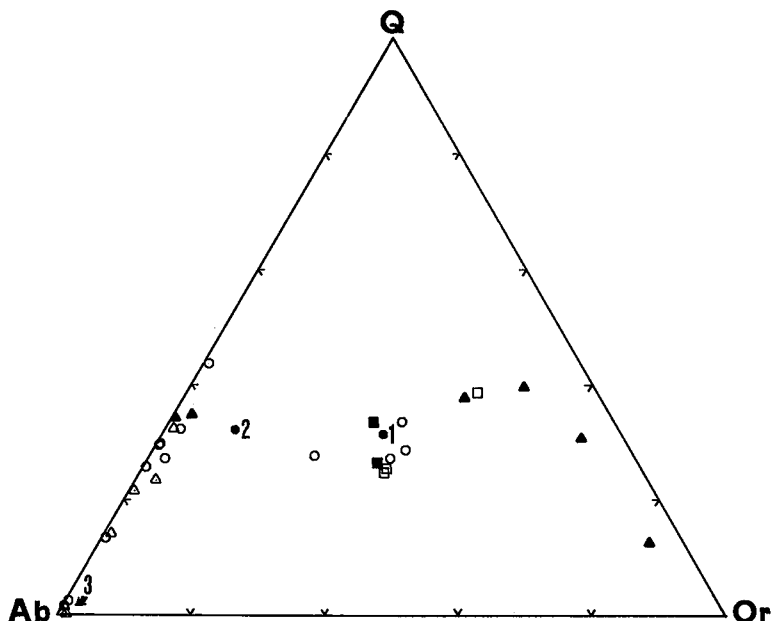


FIG. 12. Triangular plot showing normative Q, Ab and Or in the rhyolitic tuffs and porphyritic rhyolites. Open circles: Gandhi (1978); triangles: tuffs (this study); squares: porphyritic rhyolite (this study). Rare-earth analyses are presented in Table 4 for specimens shown by a full square or triangle. The average compositions of Michelin ignimbritic rocks (Table 5) are shown by black dots [1 nonmineralized ignimbrites, 2 mineralized tuffs away from the ore zone, 3 (arrow for clarity) metasomatized tuffs in the ore zone].

inference drawn previously from alkali feldspar cell parameters. Note that the three cases of important K-metasomatism (W1, W7 and W37) are now subalkaline; they have agpaite indices of 0.95, 0.83 and 0.96, respectively. Yet their microclines seem to indicate interaction with a peralkaline medium. We tentatively suggest that some rocks shown in the subalkaline field in Figure 13, to the left of the vertical line  $Na + K = Al$ , are not now as alkaline as they once were. The same could be proposed to account for banded rhyolitic tuff W47 (agpaite index 0.95), which contains relics of aegirine-augite. Removal of alkalis most probably occurred during the waning stages of deuteric hydrothermal circulation, but could have recurred at any time thereafter, for example, during an orogeny (Hudsonian, Grenville or both).

Considering the rhyolitic compositions close to the centre of Figure 12, which are presumably not too far removed from the original products of magmatic crystallization, we note that most are marginally subalkaline. They bear the ear-

marks of nonorogenic rhyolites: relatively low Ca, Mg and Al and relatively high Na, K and Fe. These trends become highly modified during the superimposed autometasomatic phenomena that accompany the cooling of the volcanic pile. Figure 12 also shows that compositional disturbances may range from subtle to extreme, the extreme cases resulting from the relatively efficient infiltration and permeation of alkaline fluids through the tuffs. Gandhi (1978) did remark that "the mineralized zones in rhyolites...have some features similar to those of fenitized rocks". The major-element trends recorded are indeed those noted in well-documented cases of fenitization: (1) strong desilication, (2) disturbance in the alkalis and (3) buildup in total iron and progressive oxidation of iron.

#### *Uranium and thorium*

As the trend of progressive desilication is dominant among this suite of felsic rocks, we have chosen to illustrate the mobility of se-

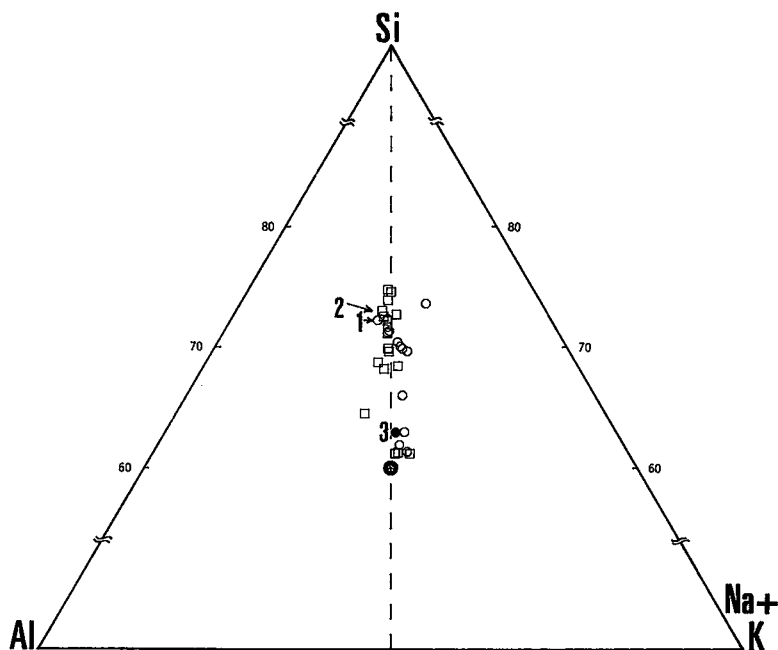


FIG. 13. Triangular plot showing atomic proportions of Si, Al and Na+K. The vertical line expresses the relationship  $\text{Na} + \text{K} = \text{Al}$ . Open circles: Gandhi (1978); squares: tuffs and porphyritic rhyolites investigated in this study. The average compositions of Michelin ignimbritic rocks (Table 5) are labeled 1, 2 and 3; 1 (nonmineralized ignimbrites) and 2 (mineralized tuffs away from the ore zone) plot to the right of the arrow but to the left of the vertical line, whereas 3 (metasomatized tuffs in the ore zone) is shown by a black dot. The star indicates the position of albite ( $\text{An}_0$ ) and microcline.

lected minor elements as a function of number of Si cations *per* 100 oxygens. In such diagrams, commonly used in studies of fenites, quartz would plot at  $Si = 50$ ; the Aillik rocks range in  $Si$  from 42.2 to 34.4. Relevant data are taken from Table 3 and from Gandhi (1978, Table 1).

Despite considerable scatter among the data points (coefficient of correlation  $r^2 = 0.34$ , considered significant using Fischer's ratio, in view of the number of data points), the concentration of uranium seems to increase with progressive desilication of the Aillik rocks (Fig. 14). Note that one exceptional rhyolite specimen ( $Si = 41.8$ ) contains 1350 ppm U, and that not all desilicated rocks are strongly enriched in uranium. The tuffaceous specimens taken from the ore zone at Michelin are among the most Si-depleted rocks of the suite. The distribution of data points for thorium (Fig. 15) is also rather scattered, but suggests an antithetic pattern to

that of uranium. The most siliceous rocks of the suite contain close to 30 ppm Th; except for three anomalously high values (only one of which occurs in a uranium-rich, Si-depleted specimen), there seems to be a progressive decrease in thorium concentration with decreasing  $Si$  value. The antithetic relationship between U and Th conflicts with the trends found in many suites of very fresh volcanic rocks, in which processes of crystal fractionation are the dominant cause of observed patterns of incompatible element buildup (*e.g.*, Smith & Bailey 1966, Cheminée 1973).

As progressive desilication of the tuffs and rhyolites is accompanied by major disturbance in the proportion of the two major alkali cations, we present in Figure 16 a plot of the relationship  $U/(U + \text{Th})$  versus  $\text{Na}/(\text{Na} + \text{K})$ . The rocks with the most closely pristine magmatic compositions are characterized by  $\text{Na}/(\text{Na} + \text{K})$  ratios close to 0.52. Note that in

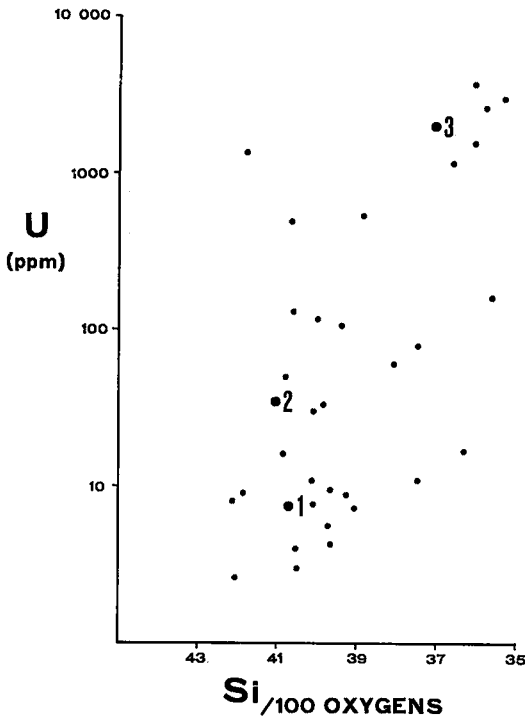


Fig. 14. U (ppm) versus Si, the number of Si cations per 100 oxygens. Points 1, 2 and 3 as in Figure 12.

such rocks,  $U/(U + Th)$  is low, ranging from 0.1 to 0.3. Nothing changes in this ratio as a result of K-metasomatism, perhaps because the temperatures involved are not sufficiently high to selectively mobilize Th and the pH range is too low to complex U. However, as a result of Na-metasomatism, U very clearly shows a progressive enrichment; values of  $U/(U + Th)$  increase steadily from 0.35 to 1.0. Note that there is a very clean separation between "pristine" and Na-metasomatized rocks, but that there is a continuum in  $U/(U + Th)$  ratios. Uranium and sodium seem to exhibit parallel developments in this hydrothermal system, but the response of uranium is more sluggish (U is less mobile?) than that of sodium.

#### Zirconium, lead and copper

Zirconium is an element that is normally strongly concentrated in residual silicate melts, such that the most silicic differentiates contain the most Zr (e.g., Barberi *et al.* 1975). The pattern shown in Figure 15 is clearly the reverse: the highest Zr values occur in the least

siliceous samples. Also, the high values occur in rocks that are clearly peralkaline (A.I. > 1.0). We contend that the buildup in Zr reflects the relatively improved mobility of this "inert" element by the high-pH fluids that caused efficient Na-metasomatism and the removal of Si.

Interestingly, the distribution of Pb (Fig. 15) is similar; it is strongly skewed, uniformly low in most rocks and highly enriched in the tuffs poorest in Si. Lead, like zirconium, is a residual element in evolved silicate melts, normally concentrated in the most fractionated products of an igneous suite. There is strong negative correlation between Pb and S (see below), suggesting that the lead is also mobilized by the dominant anions in the peralkaline fluid phase. In contrast, copper is generally removed with progressive desilication (Fig. 15). The positive correlation between Cu and S suggests that both were removed during Na-metasomatism, possibly together in a soluble complex.

#### The rare earths

The rare earths show evidence of limited mobility during these bulk-composition changes. The data, obtained by neutron-activation procedures, are presented in Table 4 and are shown in a chondrite-normalized plot (Fig. 17) separately for K-metasomatized and Na-metasomatized specimens (the pattern for W35, judged to have retained closely its primary bulk composition, is shown twice for reference). Unfortunately, the strongly Na-metasomatized, desilicated and mineralized tuffs Or 81, 82 and 83, which contain 530, 1180 and 1550 ppm U, respectively, could not be analyzed for rare earths by neutron activation because of interferences. In Figure 17, Gd concentrations are inferred by drawing Sm, Gd and Tb collinearly on the chondrite-normalized plot.

The three specimens chosen to illustrate the trend of Na-metasomatism and mild desilication (in the sequence W49b, 350a and 315) show a very similar rare-earth pattern to that of W35. All are characterized by marked light-rare-earth enrichment and negative Eu anomalies. All three "disturbed" specimens show a more pronounced Eu anomaly than W35. Interestingly, the specimen most enriched in light and heavy rare-earths and most depleted in Eu (315) is the only one plotted that is peralkaline. A different analytical technique would have to be used to test the discovery by McLennan & Taylor (1979) that U mineralization is accompanied by massive buildup in REE, especially the heavy lanthanides.

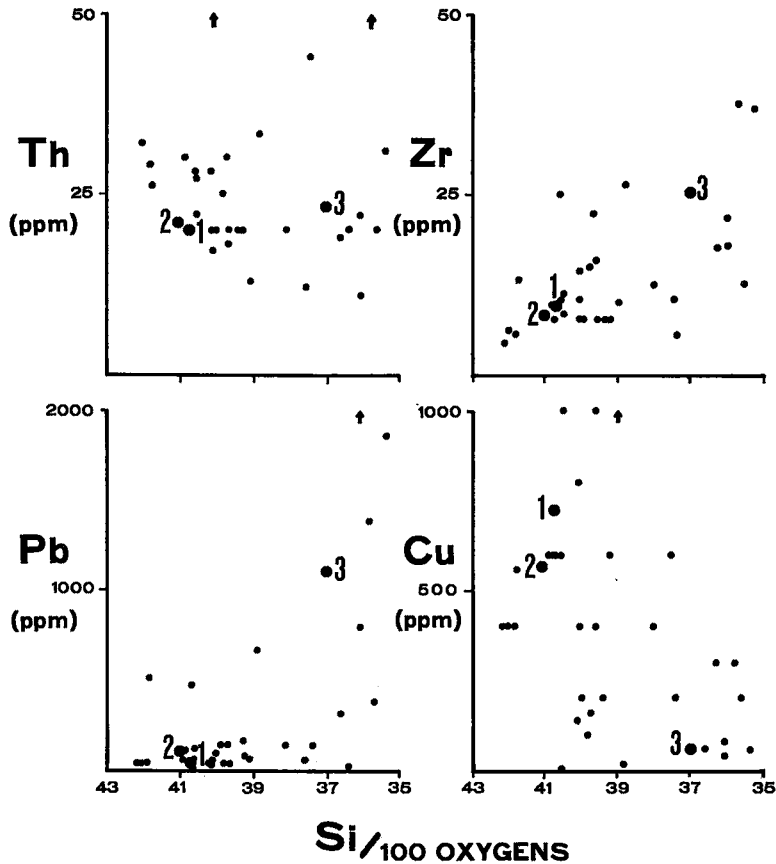


FIG. 15. Th, Zr, Pb and Cu (ppm) versus Si, the number of Si cations per 100 oxygens. Points 1, 2 and 3 as in Figure 12.

In comparison with the same reference specimens, the K-metasomatized rocks show lower light-rare-earth concentrations and considerably steeper negative Eu anomalies. However, the overall differences between Na- and K-rich suites are not striking; metasomatism seems to have amplified pre-existing magmatic trends, which indicate significant plagioclase fractionation, a dominant process that contributed to the evolution of these nonorogenic differentiates from a gabbroic parent magma (Martin & Piwinski 1974).

#### The anions

Analytical results available for S, Cl, CO<sub>2</sub> and F are plotted as a function of Si per 100 oxygens in Figure 18. As noted in a discussion of the distribution of copper in these rocks, sulfur generally attains higher levels in the siliceous rocks and is depleted in the desilicated, urani-

um-enriched tuffs. In contrast, CO<sub>2</sub>, Cl and, somewhat less convincingly, F show progressive increases with increasing desilication. These plots provide clear evidence of the importance of the carbonate anion in the alkaline fluid phase that effected the metasomatic changes and transported uranium. McLennan & Taylor (1979) also noted this correlation and proposed a soluble uranyl carbonate complex such as [UO<sub>2</sub>(CO<sub>3</sub>)<sub>3</sub>]<sup>4-</sup> to account for uranium transport in alkaline environments. Gabelman (1977), Romberger (1978) and Hambleton-Jones (1978) reviewed the evidence for urano-halogen complexes; in the light of their comments, fluorine probably also was involved in U transport in the Michelin deposits, but the role of chlorine may have been insignificant.

#### Summary

For the Michelin deposit, a summary state-

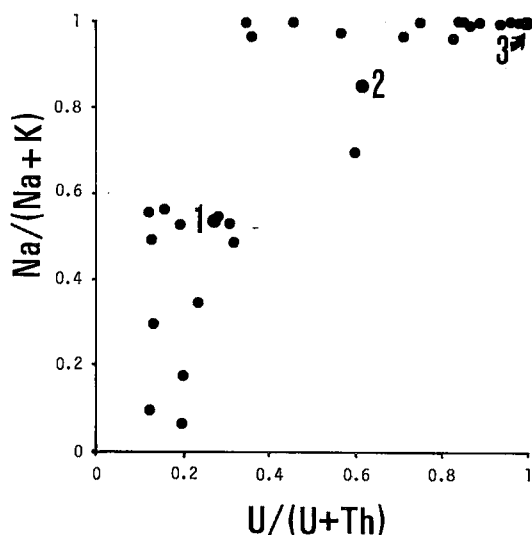


Fig. 16.  $\text{Na}/(\text{Na}+\text{K})$  versus  $\text{U}/(\text{U}+\text{Th})$  in rhyolitic rocks of the Upper Aillik Group. Data are taken from Gandhi (1978) and from Table 3. Points 1, 2 and 3 as in Figure 12.

ment of the chemical changes that have been discussed, based in part on the data in Table 3 and in part on unpublished analyses, is provided by the three average compositions listed in Table 5. The average nonmineralized Michelin ignimbrite represents X-ray-fluorescence analyses of 34 specimens from section M31 (Fig. 1). These average compositions are shown in Figures 12 to 16 and in Figure 18.

#### DISCUSSION

In the Aillik Group, the pillowed basic volcanic rocks of the lower division and the dominantly felsic products (tuffs and shallow intrusive rocks) of the upper division seem to define a bimodal suite. This is also reflected in

TABLE 4. RARE-EARTH-ELEMENT DATA FOR SELECTED TUFFACEOUS AND PORPHYRITIC RHYOLITES OF THE AILLIK GROUP

Spec.	U	Th	La	Nd	Sm	Ce	Eu	Tb	Yb	Lu	Sc
315	16	30	184	144	20.1	277	0.7	1.7	8.7	1.4	2
350a	130	27	127	110	22.0	182	1.4	1.6	4.0	---	5
W37	8	32	98	83	14.6	159	0.4	1.5	6.8	1.0	1
W47	9	29	106	85	13.0	132	0.7	1.7	6.5	0.9	2
W1	4	28	94	75	11.2	134	1.1	1.2	5.1	0.7	3
W35	3	22	134	114	17.1	195	1.9	1.6	6.2	0.9	3
W49b	11	28	75	65	11.8	96	1.0	1.4	7.1	1.1	4
W7	11	44	134	99	14.3	145	0.6	1.4	7.2	1.1	4

Concentrations in ppm; data obtained by neutron-activation techniques by X-Ray Assay Laboratories, Ltd. Rare-earth data could not be obtained on the following specimens of uranium-enriched tuffs: Or81 (530 ppm U, 37 ppm Th, 9 ppm Sc), Or82 (1180 ppm U, 16 ppm Th, 4 ppm Sc) and Or83 (1550 ppm U, 9 ppm Th, 6 ppm Sc).

composite dykes of coarse rhyolite porphyry rimmed by narrow basic margins, observed in the Wild Bight coastal section (see Gandhi 1978, Fig. 23). Among dozens of analyses of volcanic rocks reported by Watson-White (1976; specimens from the Kitts - Post Hill belt as well as the area discussed here), a gap between 52 and 68 wt. %  $\text{SiO}_2$  is occupied by a single specimen containing 58%. A number of geochemical indicators suggest that the basalts are transitional to mildly alkaline. In composition and mineralogy, the undisturbed felsic differentiates in the Aillik resemble nonorogenic granitic liquids formed at high crustal levels (Martin & Piwinski 1972). These lines of evidence suggest strongly that the Aillik Group volcanic and shallow plutonic rocks define a rift-related suite.

Our inference of a classic case of nonorogenic volcanism, which rests on geochemical and mineralogical arguments, contradicts the opinion of a number of recent investigators. Wardle & Bailey (1980) suggested that the transition from basic volcanism in the Lower Aillik to felsic volcanism in the Upper Aillik indicates the onset of radically different tectonic conditions, from rifting to ensialic orogeny. Our data, admittedly based on a restricted geographical coverage of the Upper Aillik, are inconsistent with their proposal of a calc-alkaline character for these rocks. Pseudo-calc-alkaline compositions could arise during the metasomatic overprints. In our opinion, the rhyolites must be preorogenic, not synorogenic.

To Kontak *et al.* (1980b), the voluminous amount of rhyolite, its peraluminous character where sampled, its potassic character and "moderate to high" initial  $^{87}\text{Sr}/^{86}\text{Sr}$  ratios (maximum 0.7070) suggest a crustal source for the upper part of the Aillik Group. The first characteristic is commonly encountered in the classical nonorogenic suites, even those found far from a sialic basement. We contend that the local enrichment in K and the appearance of peraluminous characteristics are not features that pertain to the original magma in this case, but that emerge at the postmagmatic stage. These deuteric modifications should be revealed clearly in the textures of the alkali feldspars. Where the exsolution textures are strongly modified, as documented in this investigation, no inference may be made about magma composition from rock compositions encountered. Finally, the initial  $^{87}\text{Sr}/^{86}\text{Sr}$  ratio is greatly susceptible to resetting to higher values, because nonorogenic felsic liquids, believed to have

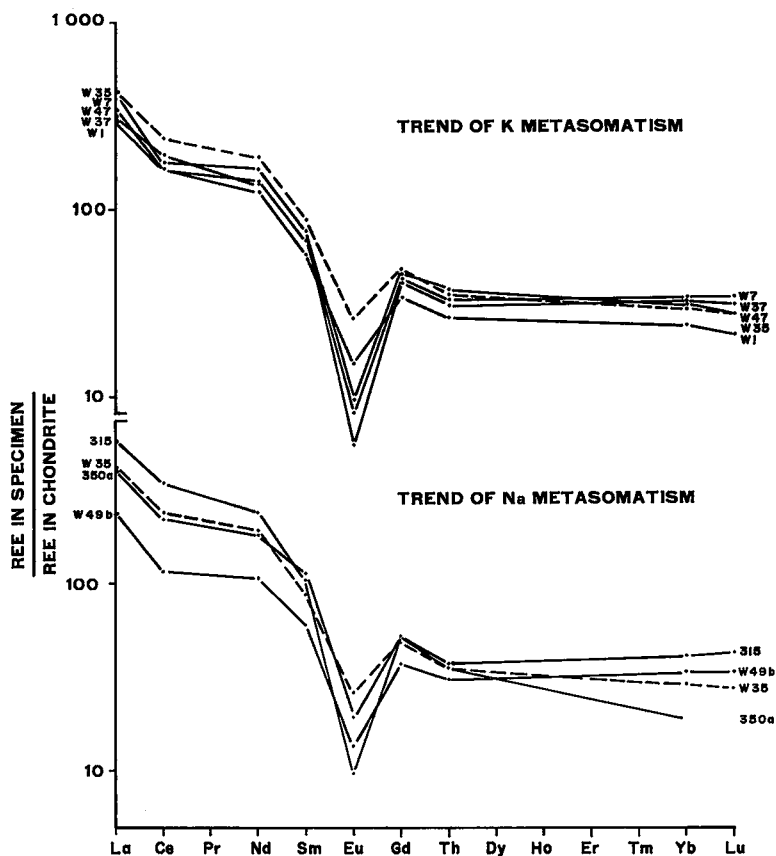


FIG. 17. Rare-earth-element plots (chondrite-normalized) for the rocks indicated in Figure 12. These are shown in two sequences, one of progressive K-metasomatism (top), the other showing Na-metasomatism. The values recommended by G. Goles (priv. comm. 1980) are used as normalization factors.

fractionated from a gabbroic parent (Martin & Piwinski 1974), contain very low concentrations of Sr; furthermore, most of this Sr is located in feldspar, which is undergoing profound modifications. If the fluids that catalyze these changes encounter Archean basement in their path of circulation during the deuterian events, selective contamination of the differentiates in  $^{87}\text{Sr}$  will be the expected phenomenon. Martin & Bowden (1981) explore the importance of these deuterian transformations in a study of the origin of peraluminous granites in the nonorogenic Ririwai ring complex, Nigeria.

The fractionated members of nonorogenic igneous complexes are strongly enriched in incompatible elements. These most probably increased upward in the holding reservoir in which differentiation processes were at work. Smith & Bailey (1966), Locardi (1967), Chemi-

née & Nougier (1972), Cheminée (1973) and Barberi *et al.* (1975) showed in numerous examples that at the magmatic stage, the increase in U and Th contents follows that of K. Material in the ash-fall deposits, generated as products of a Plinian eruption, probably was tapped from this enriched roof zone of the chamber. These glass-rich, fine-grained deposits were easily eroded, and could have been re-sedimented in adjacent subaqueous environments. Material in ash-flow deposits probably originated from deeper but still volatile-rich parts of the reservoir that were also notably enriched in incompatible elements like U and Th. The pile of tuffaceous rhyolitic products was then intruded by domes of relatively degassed  $\beta$ -quartz-, feldspar-phyric obsidian. Unfortunately, structural disruptions due to later orogenies prevent reconstruction of the immediate post-

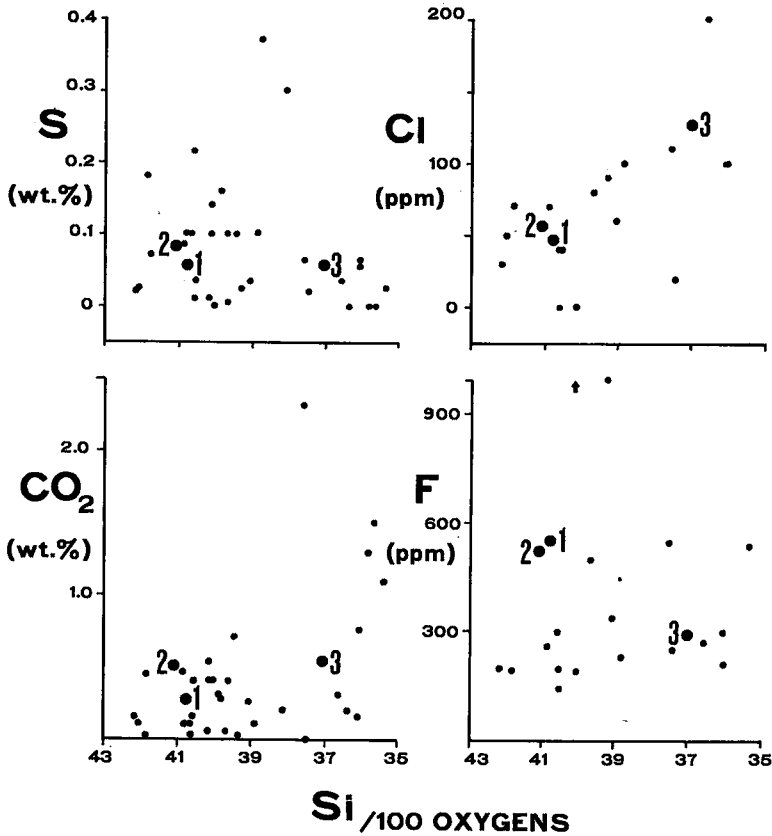


Fig. 18. S (wt. %), Cl (ppm), CO<sub>2</sub> (wt. %) and F (ppm) plotted as a function of Si, the number of Si cations per 100 oxygens. Points 1, 2 and 3 as in Figure 12.

eruption events and geometries. By analogy with modern examples, however, considerable element mobility is expected to have occurred as the massive ignimbritic deposits became compacted (locally welded) and expelled water. As the rocks were mildly alkaline, the fluid phase so expelled also must have had an alkaline character. It is at this stage that U and Th may have become separated.

A removal of Na without loss of Si seems to have occurred in parts of the pile of tuffaceous material, whereas elsewhere it was K and, eventually, Si that were removed as Na was added. One way of explaining these contrasting metasomatic trends is to propose that convection cells were set up in the tuffs, possibly controlled by the intrusive plugs and vent systems that provided local heat sources. The primary elemental buildup patterns would very likely be disturbed during these deuteric events, with the extent of disturbance clearly depending

mostly on permeability of the rocks and their grain size. Minimal effects are shown in uniformly medium-grained rocks. Where porphyritic textures are well developed, the fine-grained groundmass invariably shows more profound disturbances than the phenocrysts (Fig. 10). The most extreme effects are shown in uniformly very fine-grained rocks; the feldspar mineralogy of these aphanitic assemblages provides valuable insight into the progression of these surface-controlled reactions.

The circulating, mildly alkaline fluid medium interacted with the rocks at a variety of temperatures. We contend that in low-temperature dissolved preferentially over Th, presumably parts of the convection system, uranium was as a sodium-bearing uranyl carbonate or halide complex; in these parts of the system, the sodium removed was replaced by potassium in the feldspar structure via an ion-exchange reaction. The microcline attained very high de-

TABLE 5. AVERAGE COMPOSITIONS OF MICHELIN IGNI-MBRITIC ROCKS

	1	2	3
SiO <sub>2</sub> %	74.0 ± 2.2	75.0 ± 2.2	65.8 ± 2.2
TiO <sub>2</sub>	0.32 ± 0.12	0.26 ± 0.10	0.52 ± 0.20
Al <sub>2</sub> O <sub>3</sub>	12.5 ± 0.74	12.2 ± 0.35	16.3 ± 1.5
FeO <sup>v</sup>	3.04 ± 1.03	2.61 ± 0.70	4.61 ± 0.85
MnO	0.04 ± 0.01	0.04 ± 0.03	0.08 ± 0.03
MgO	0.19 ± 0.14	0.21 ± 0.20	0.33 ± 0.29
CaO	1.11 ± 0.43	0.89 ± 0.21	2.02 ± 0.72
Na <sub>2</sub> O	3.83 ± 0.67	6.14 ± 1.8	10.1 ± 1.3
K <sub>2</sub> O	4.99 ± 0.69	1.66 ± 0.26	0.11 ± 0.03
P <sub>2</sub> O <sub>5</sub>	0.03 ± 0.02	0.03 ± 0.02	0.08 ± 0.05
Fe/Mg	16	12	14
K/(K+Na)	0.57	0.21	0.01
U ppm	7.4 ± 2.3	34 ± 39	1900 ± 1400
Th	20 ± 3.8	21 ± 5.3	23 ± 7
Cl	46 ± 35	54 ± 43	125 ± 50
F	550 ± 450	520 ± 600	290 ± 130
S	550 ± 360	820 ± 630	560 ± 290
CO <sub>2</sub> %	0.27 ± 0.17	0.50 ± 0.69	0.54 ± 0.41
Th/U	2.7	0.62	0.01
Cu ppm	36 ± 36	23 ± 14	3 ± 2
Pb	39 ± 32	49 ± 18	550 ± 420
Zn	81 ± 35	68 ± 20	64 ± 68
Zr	375 ± 105	340 ± 62	1020 ± 330
Enrichment	CO <sub>2</sub> , Ca, U, S	Na, CO <sub>2</sub> , U	Ca, Mg, Na, Fe, Ti, P, U, Cl, Pb, Zr
Depletion		K	Si, K, Cu

<sup>v</sup> total Fe expressed as FeO. 1. Average composition of non-mineralized Michelin ignimbrite ( $n = 34$ ), taken from section M31 (Fig. 1). 2. Average composition of mineralized tuffs away from the ore zone ( $n = 9$ ); specimens 301, 302, 303, 304, 306, M<sub>1</sub>66, 312, 315, 317. 3. Average composition of metasomatized tuffs in the ore zone ( $n = 6$ ), based on the Or series of specimens. Individual rocks analyses of 313, 315, M31-350a, Or80, Or81, Or82, Or83 and Or84 are presented in Table 3. Ranges reflect  $\pm 1\sigma$ .

degrees of Si-Al order in this alkaline environment, so that temperatures were still appropriate (tentatively,  $> 200^\circ\text{C}$ ) for the solution-and-re-deposition steps involved in Si-Al ordering. In higher-temperature parts of the system, the uranium was precipitated, owing to breakdown of the soluble complex and reduction of pH or of  $\text{P}(\text{O}_2)$  in the fluid medium, possibly as a result of nearby oxidation in the metasomatic envelope (Evans 1980). Gandhi (1978) favors an overall reducing environment in view of the occurrence of graphite and pyrrhotite in mineralized zones. One could also postulate that the formation during metasomatism of sodic pyroxenes and amphiboles (e.g., Gandhi 1978, Table 1, anal. 15, 16) and the possible early deposition of U as pyrochlore in zones of Na-metasomatism led to a significant reduction in pH. The fact that the albites are not unusually well ordered in the ultrasodic rocks (Fig. 11) is consistent with a marked decrease in alkalinity of the fluid medium. Also, at the time of active metasomatism by the carbonate-bearing aqueous fluid, some calcium may have been incorporated into the feldspar structure. This would imply temperatures above the upper limits of the

greenschist facies. Finally, as the solubility of quartz increases with increasing temperature (e.g., Walther & Helgeson 1977), the efficient desilication noted in the Na-metasomatized tuffs (now albitites) is consistent with a relatively high-temperature precipitation of the uranium (cf., Romberger 1978).

The size of the convection cell(s) in the accumulation of tuffaceous rocks remains unknown. It is clear that units of similar enrichment pattern may be spatially related. East of Mustang Lake (Fig. 1), a sodium-enriched rhyolite porphyry plug that occupies a probable feeder is contiguous to a strongly sodium-enriched banded rhyolitic tuff of ash-flow origin (W39); both are mildly peralkaline. Similarly, the potassium-enriched felsic dyke W7 occurs near a K-rich banded ash-flow rhyolitic sequence (specimen W1) east of Walker Lake, approximately 5 km NW of the Michelin showings. The sample density in this investigation is insufficient to comment further on the size of the hydrothermal convection systems and their polarity. The Na-U geochemical coherence in this volcanic belt and in many other occurrences (e.g., MacKevett 1963, Kazanskii *et al.* 1968, Hoeve 1974, Jacobson & MacLeod 1977) is striking; it would seem a very worthwhile exploration tool to establish the regional patterns of alkali enrichment in volcanic and related sedimentary units in areas of suspected remobilization of uranium and other incompatible elements.

The following features, considered significant and taken collectively, account for the economic potential of the Central Mineral Belt: (1) the parental igneous suite is mildly alkaline and inferred to be rift-related. Sørensen (1977) has pointed out that primary concentrations of U, Th and other incompatible elements in the melt are greater the greater its alkalinity. (2) The igneous complex was shallow, possibly related to a large epizonal granitic pluton. The Walker Lake granite contains porphyritic variants that seem to grade into quartz feldspar porphyry (Smyth 1977). Bailey (1978) also considered the possibility that the Walker Lake pluton is comagmatic with the rhyolites, though on face value, the published isochron would rule out this possibility. (3) The ash was composed largely of glass shards and pumice fragments. Uranium can be removed efficiently by alkaline solutions if the matrix is vitreous (Zielinski 1979). The U, Th and associated suite of elements were perhaps also efficiently mobilized when the glass eventually devitrified to a

quartzofeldspathic assemblage. (4) A mildly alkaline aqueous fluid was set in motion near the intrusive plugs and around the perimeter of the inferred subjacent pluton. Fluids encountered relatively cool rocks in their path; it is here that U was dissolved, perhaps principally as a uranyl carbonate or halide complex. However, these fluids could also migrate to hotter parts of the system, perhaps areas of thick ash-flow accumulations of rhyolitic pumiceous material undergoing welding. It is here, and perhaps in zones of mostly vertical flow (Fehn *et al.* 1978) that deposition occurred from the fluid in response to changes in important intensive variables. (5) In view of the occurrences of uranium mineralization along well-defined shear zones, Bailey (1978) concluded that remobilization of uranium along faults had occurred, either during or after shearing. (6) Finally, distinctly later events (poly-phase deformation, contact-metamorphic effects associated with post-Hudsonian intrusive activity) may have provided further opportunities for concentration of the selectively mobile elements.

#### ACKNOWLEDGEMENTS

We are grateful to Brinco Ltd. for logistical support in the field and for assistance during this project. R.F. Martin acknowledges the insight provided by Dr. R.O. Fournier, U.S. Geological Survey, Menlo Park, California. We thank Ms. S. Horsky, now at the University of British Columbia, Mr. Yves Lalonde (Université de Montréal), Ms. V. Trimarchi and Mr. R. Yates (both at McGill) for help in the preparation of this report. Many analyses and all X-ray-diffraction studies were funded by a grant from the Natural Sciences and Engineering Research Council (A7721) to RFM. Associate editor L.T. Trembath and two anonymous reviewers provided very helpful suggestions.

#### REFERENCES

- APPLEMAN, D.E. & EVANS, H.T., JR. (1973): Job 9214: indexing and least-squares refinement of powder diffraction data. *U.S. Geol. Surv. Comp. Contr.* 20.
- BACHINSKI, S.W. & MÜLLER, G. (1971): Experimental determinations of the microcline-low albite solvus. *J. Petrology* 12, 329-356.
- BAILEY, D.G. (1978): The geology of the Walker Lake — MacLean Lake area (13K/9, 13J/12), Central Mineral Belt, Labrador. *In Report of Activities for 1977* (R.V. Gibbons, ed.), *Nfld. Dep. Mines Energy Rep.* 78-1.
- , FLANAGAN, M.J. & LALONDE, A. (1979): Geology of eastern Central Mineral Belt (13J/10-15; 13O/2,3), Labrador. *In Report of Activities for 1978* (R.V. Gibbons, ed.), *Nfld. Dep. Mines Energy Rep.* 79-1.
- BARBERI, F., FERRARA, G., SANTACROCE, R. TREUIL, M. & VARET, J. (1975): A transitional basalt-pantellerite equence of fractional crystallization, the Boina centre (Afar rift, Ethiopia). *J. Petrology* 16, 22-56.
- BLASI, A. (1977): Calculation of T-site occupancies in alkali feldspar from refined lattice constants. *Mineral. Mag.* 41, 525-526.
- CHEMINÉE, J.-L. (1973): *Contribution à l'Étude des Comportements du Potassium, de l'Uranium et du Thorium dans l'Évolution des Magmas*. D. ès Sc. thesis. Univ. Paris VI. France.
- & NOUGIER, J. (1972): Distribution of uranium, thorium and potassium in the volcanic suites of Iles Kerguelen. *In Antarctic Geology and Geophysics* (R.J. Adie, ed.), Universitetsforlaget. Oslo, Norway.
- CLARK, A.M.S. (1971): Structure and lithology of a part of the Aillik series, Labrador. *Geol. Assoc. Can. Proc.* 24, 107-117.
- (1979): Proterozoic deformation and igneous intrusions in part of the Makkovik sub-province, Labrador. *Precambrian Res.* 10, 95-114.
- EVANS, D.F. (1980): *Geology and Petrochemistry of the Kitts and Michelin Uranium Deposits and Related Prospects, Central Mineral Belt, Labrador*. Ph.D. thesis, Queen's Univ., Kingston, Ontario.
- FEHN, U., CATHLES, L.M. & HOLLAND, H.D. (1978): Hydrothermal convection and uranium deposits in abnormally radioactive plutons. *Econ. Geol.* 73, 1556-1566.
- GABELMAN, J.W. (1977): Migration of uranium and thorium — exploration significance. *Amer. Assoc. Petroleum Geol., Stud. Geol.* 3.
- GANDHI, S.S. (1978): Geological setting and genetic aspects of uranium occurrences in the Kaipokok Bay — Big River area, Labrador. *Econ. Geol.* 73, 1492-1522.
- GOWER, C.F. (1980): Geology of the Benedict Mountains and surrounding areas 13J (east half) and 13I, Labrador. *In Current Research* (C.F. O'Driscoll & R.V. Gibbons, eds.), *Nfld. Dep. Mines Energy Rep.* 80-1, 182-191.
- HAMBLETON-JONES, B.B. (1978): Theory and practice of geochemical prospecting for uranium. *Minerals Sci. Eng.* 10, 182-197.

- HOEVE, J. (1974): *Soda Metasomatism and Radioactive Mineralization in the Västervik Area, Southeastern Sweden*. Ph.D. thesis, Free Univ., Amsterdam, The Netherlands.
- JACOBSON, R.R.E. & MACLEOD, W.N. (1977): Geology of the Liruei, Banke and adjacent younger granite ring-complexes. *Geol. Surv. Nigeria Bull.* **33**.
- KAZANSKII, V.I., KRUPENIKOV, V.A., OMEL'YANENKO, B.I. & PRUSS, A.K. (1968): Structural and petrological conditions for the formation of uraniumiferous albitites. *Geol. Rudn. Mesterozhd.* **10**(1), 3-16 (in Russ.).
- KONTAK, D.J., MORTON, R.D. & BAADSGAARD, H. (1980a): Recognition of uraniumiferous sub-provinces within the Central Mineral Belt of southern Labrador, Canada. *Geol. Assoc. Can./Mineral. Assoc. Can. Program Abstr.* **5**, 66.
- , ——— & ——— (1980b): Geology, Rb/Sr geochronology, and geotectonics of the Central Mineral Belt, southern Labrador. *Geol. Assoc. Can./Mineral. Assoc. Can. Program Abstr.* **5**, 66.
- LOCARDI, E. (1967): Uranium and thorium in the volcanic processes. *Bull. Volc.* **31**, 235-260.
- LOFGREN, G. (1970): Experimental devitrification rate of rhyolite glass. *Geol. Soc. Amer. Bull.* **81**, 553-560.
- (1971): Experimentally produced devitrification textures in natural rhyolitic glass. *Geol. Soc. Amer. Bull.* **82**, 111-124.
- MACKEVETT, E.M., JR. (1963): Geology and ore deposits of the Bokan Mountain uranium-thorium area, southeastern Alaska. *U.S. Geol. Surv. Bull.* **1154**.
- MARTEN, B.E. (1977): *The Relationship Between the Aillik Group and the Hopedale Complex, Kaipokok Bay, Labrador*. Ph.D. thesis, Memorial Univ. of Newfoundland, St. John's.
- MARTIN, R.F. (1974): Controls of ordering and subsolidus phase relations in the alkali feldspars. In *The Feldspars* (W.S. MacKenzie & J. Zussman, eds.), *Proc. NATO Advanced Study Inst.*, Manchester Univ. Press, Manchester, England.
- (1977): The association hypersolvus granite-subsolvus granite-"solvbergite" at Andrew's Point, Cape Ann, Massachusetts: a case of localized fenitization. *Amer. J. Sci.* **277**, 273-287.
- & BOWDEN, P. (1981): Nonorogenic peraluminous granites in the Ririwai ring-complex, Nigeria. *Can. Mineral.* **19**, (in press).
- & PIWINSKII, A.J. (1972): Magmatism and tectonic settings. *J. Geophys. Res.* **77**, 4966-4975.
- & ——— (1974): The contrasting origin of orogenic and non-orogenic granitoid rocks. In *Proc. Symp. Andean and Antarctic Volcanology Problems* (O. Gonzales-Ferran, ed.), *Int. Assoc. Volc. Chem. Earth's Interior*.
- MCLENNAN, S.M. & TAYLOR, S.R. (1979): Rare earth element mobility associated with uranium mineralisation. *Nature* **282**, 247-250.
- MCMILLAN, R.H. (1978): Genetic aspects and classification of important Canadian uranium deposits. *Mineral. Assoc. Can. Short Course Handbook* **3**, 187-204.
- MINATIDIS, D.G. (1976): *A Comparative Study of Trace Element Geochemistry and Mineralogy of some Uranium Deposits of Labrador, and Evaluation of some Uranium Exploration Techniques in a Glacial Terrain*. M.Sc. thesis, Memorial Univ., St. John's, Nfld.
- POULIOT, G. (1968): Paramorphisme du quartz dans le granophyre de l'intrusion de Muskox, T.N.O. *Naturaliste can.* **95**, 1277-1292.
- ROMBERGER, S.B. (1978): Hydrothermal transport and deposition of uranium, and the origin of vein uranium deposits. *Geol. Soc. Amer. Abstr. Program* **10**, 480.
- SIEMIATKOWSKA, K.M. & MARTIN, R.F. (1975): Fenitization of Mississagi quartzite, Sudbury area, Ontario. *Geol. Soc. Amer. Bull.* **86**, 1109-1122.
- SMITH, J.V. (1974): *Feldspar Minerals. 1. Crystal Structure and Physical Properties*. Springer-Verlag, New York.
- SMITH, R.L. & BAILEY, R.A. (1966): The Bandelier tuff: a study of ashflow eruption cycles from zoned magma chambers. *Bull. Volc.* **29**, 83-104.
- SMYTH, W.R. (1977): The geology of the Stiepec Lake - Walker Lake area, Central Mineral Belt, Labrador. In *Report of Activities for 1976* (R.V. Gibbons, ed.), *Nfld. Dep. Mines Energy Rep.* **77-1**.
- SØRENSEN, H. (1977): Features of the distribution of uranium in igneous rocks - uranium deposits associated with igneous rocks. In *Recognition and Evaluation of Uraniferous Areas*. *Int. Atomic Energy Agency, Vienna*.
- SPARKS, R.S.J., SELF, S. & WALKER, G.P.L. (1973): Products of ignimbrite eruptions. *Geology* **1**, 115-118.
- STEVENSON, J.S. (1963): The upper contact phase of the Sudbury micropegmatite. *Can. Mineral.* **7**, 413-419.

- STEWART, D.B. & RIBBE, P.H. (1969): Structural explanation for variation in cell parameters of alkali feldspar with Al/Si ordering. *Amer. J. Sci.* 267A, 444-462.
- & WRIGHT, T.L. (1974): Al/Si order and symmetry of natural alkali feldspars, and the relationship of strained cell parameters to bulk composition. *Soc. franç. Minéral. Crist. Bull.* 97, 356-377.
- SUTTON, J.S., MARTEN, B.E., CLARK, A.M.S. & KNIGHT, I. (1972): Correlation of the Precambrian supracrustal rocks of coastal Labrador and south-western Greenland. *Nature Phys. Sci.* 238, 122-123.
- TUTTLE, O.F. & BOWEN, N.L. (1958): Origin of granite in the light of experimental studies in the system  $\text{NaAlSi}_3\text{O}_8\text{-KAlSi}_3\text{O}_8\text{-SiO}_2\text{-H}_2\text{O}$ . *Geol. Soc. Amer. Mem.* 74.
- WAGER, L.R., WEEDON, D.S. & VINCENT, E.A. (1953): A granophyre from Coire Uaigneich, Isle of Skye, containing quartz paramorphs after tridymite. *Mineral. Mag.* 30, 263-275.
- WALTHER, J.V. & HELGESON, H.C. (1977): Calculation of the thermodynamic properties of aqueous silica and the solubility of quartz and its polymorphs at high pressures and temperatures. *Amer. J. Sci.* 277, 1315-1351.
- WARDLE, R.J. & BAILEY, D.G. (1980): Contrasting sedimentary-volcanic regimes in the Lower Proterozoic of Labrador. *Geol. Assoc. Can./Mineral. Assoc. Can. Program Abstr.* 5, 87.
- WATSON-WHITE, M.V. (1976): *A Petrological Study of Acid Volcanic Rocks in Part of the Aillik Series, Labrador*. M.Sc. thesis, McGill Univ., Montréal, Qué.
- ZIELINSKI, R.A. (1979): Uranium mobility during interaction of rhyolitic obsidian, perlite and feldspar with alkaline carbonate solution:  $T = 120^\circ\text{C}$ ,  $P = 210 \text{ kg/cm}^2$ . *Chem. Geol.* 27, 47-63.

Received May 1980, revised manuscript accepted August 1980.